



# Green synthesis of ZnO and ZnO/CuO nanocomposites in *Mentha longifolia* leaf extract: characterization and their application as anti-bacterial agents

Ramin Mohammadi-Aloucheh<sup>1</sup> · Aziz Habibi-Yangjeh<sup>2</sup> · Abolfazl Bayrami<sup>1</sup> · Saeid Latifi-Navid<sup>1</sup> · Asadollah Asadi<sup>1</sup>

Received: 4 April 2018 / Accepted: 12 June 2018 / Published online: 25 June 2018  
© Springer Science+Business Media, LLC, part of Springer Nature 2018

## Abstract

In this work, we fabricated ZnO and ZnO/CuO nanocomposites using *Mentha longifolia* leaf extract as a natural, non-toxic, and efficient stabilizer. Anti-bacterial activities of the prepared samples against two pathogenic bacteria, *Escherichia coli* (Gram-negative), and *Staphylococcus aureus* (Gram-positive) were investigated. The properties of the as-prepared samples were characterized by XRD, EDX, SEM, TEM, TGA, FT-IR, UV–Vis DRS, and BET instruments. The XRD analysis indicated that the size of crystallites was decreased for the ZnO powder prepared in the presence of the leaf extract. The SEM images showed that the samples consist of spherical shaped well-distributed particles. In addition, the presence of biomolecules from the leaf extract was revealed by EDX, TGA, FT-IR, and UV–Vis DRS analyses, which are important in biosynthesis process. The highest anti-bacterial activity belonged to the ZnO/CuO (10%) nanocomposite and the other compounds, including ZnO/CuO (5%), ZnO (ext), and ZnO (W) were in the next ranks, respectively. It was observed that the viability percentages against *E. coli* ( $10.16 \pm 2.2$ ) is higher than that of *S. aureus* ( $17.1 \pm 0.87$ ) in the presence of the ZnO/CuO (10%) nanocomposite. Ultimately, the mechanism for the action of the ZnO/CuO (10%) nanocomposite was explored through the SEM images, which involved the disruption of the bacterial membranes.

## 1 Introduction

The current attempt in nanotechnology is fabrication of nanomaterials with green procedures, unique characteristics, and high efficiency to be used in various fields [1–3]. Recently, metal oxides have been substantially used in different disciplines such as sensors, photocatalysts, UV protection, drug carriers, cosmetics, filling materials in medical industry, and anti-bacterial agents, due to offering unique properties [4]. One of these metal oxides is zinc oxide (ZnO) as a n-type semiconductor with appealing properties of green characteristics, low price, excellent stability, and existing facile preparation routes [5–8]. On the other hand, copper oxide (CuO) is another commonly used p-type semiconductor with low band gap energy, excellent chemical stability,

environmentally friendly features, anti-inflammatory, and anti-bacterial activities [9–11]. This semiconductor is one of the most attractive materials that has been widely applied in photo-electrochemical water reduction, gas sensing, catalytic activity, super-hydrophobic surfaces, solar hydrogen production, photodegradation reactions, and photovoltaic applications [12, 13].

Several physical and chemical techniques have been developed for fabrication of metal oxides including microwave-irradiation, sol–gel, chemical vapor deposition, coprecipitation, wet impregnation, and mechanical alloying methods [14–16]. Among them, microwave-irradiation route is a facile and controllable method, which has been emerged as a fast route in synthesis of organic compounds, polymers, inorganic materials, and nanomaterials [17, 18]. Green synthesis process has been accepted as a promising technique to prevail the limitations accompanied with chemical methods. This method involves the application of microorganisms, some fungus, and plants during the preparation procedure [19, 20]. The *Mentha* genus, known as “wild mint”, belongs to the family of Lamiaceae. Although this genus has spread in all parts of the earth, it has been commonly reported in Mediterranean regions, such as Australia, Europe, and North

✉ Aziz Habibi-Yangjeh  
ahabibi@uma.ac.ir

<sup>1</sup> Department of Biology, Faculty of Science, University of Mohaghegh Ardabili, P.O. Box 179, Ardabil, Iran

<sup>2</sup> Department of Chemistry, Faculty of Science, University of Mohaghegh Ardabili, P.O. Box 179, Ardabil, Iran

Africa [21–23]. Due to its tremendous properties, different parts of this plant are widely used as anti-microbial, anti-fungal, anti-spasmodic, carminative, and stimulant agents, and for treatment of various diseases such as digestive disorders and headaches. Additionally, this plant is used in the food, tobacco, and cosmetics industries [23, 24]. The known compounds in *Mentha longifolia* leaf extract are triterpenoids, steroids, beta-sitosterol, phenolic compounds, hexacosyl (*E*)-ferulate, and flavonoids. Besides, the main chemical constituents of this plant, including pulegone, menthone, isomenthone, menthol, 1,8-cineole, borneol, and piperitenone have imperative roles in different effects of this plant [24, 25]. It should be noted that the menthols are the most important components responsible for pharmacological effects of this plant [24].

In this research, ZnO powder in water, denoted as ZnO (W), in the leaf extract of *M. longifolia*, denoted as ZnO (ext), ZnO/CuO (5%), and ZnO/CuO (10%) nanocomposites were synthesized by an efficient microwave-assisted method. The phase structure, purity, morphology, thermal stability, and spectroscopic and textural properties were studied using X-ray diffraction (XRD), energy-dispersive X-ray spectroscopy (EDX), scanning electron microscopy (SEM), transmission electron microscopy (TEM), thermo gravimetric analysis (TGA), Fourier transform-infrared (FT-IR) spectroscopy, UV–Vis diffuse reflectance spectroscopy (UV–Vis DRS), and Brunauer–Emmett–Teller (BET) instruments. Additionally, to examine the anti-bacterial activities, the as-prepared materials were used against *Escherichia coli* (Gram-negative) and *Staphylococcus aureus* (Gram-positive) bacteria. The experimental results showed that the prepared samples with the leaf extract of *M. longifolia* had an excellent potential to inhibit the growth of the studied bacteria.

## 2 Experimental section

### 2.1 Materials

In this research, zinc (II) nitrate [ $\text{Zn}(\text{NO}_3)_2 \cdot 6\text{H}_2\text{O}$ ], copper (II) acetate [ $\text{Cu}(\text{CH}_3\text{COO})_2 \cdot \text{H}_2\text{O}$ ], sodium hydroxide, and ethanol with analytical grads were purchased from Merck (Darmstadt, Germany). *E. coli* (PTCC 1047) and *S. aureus* (PTCC 1189) were provided from Iranian Research Organization for Science and Technology (IROST). Nutrient broth (NB) and nutrient agar (NA) were purchased from Pronadisa (Spain).

### 2.2 Preparation of the extract

The green *M. longifolia* leaves were collected from mountainous region, the North West of Iran, Ardabil province, and

authenticated by Botanical Lab of University of Mohaghegh Ardabili, Iran. The collected green leaves were completely washed by deionized  $\text{H}_2\text{O}$  (DW) and dried at room temperature in a dust free condition for 4 days. Dried leaves were crushed into fine powder by milling. Afterward, 10 g of the powder was mixed with 100 mL DW and refluxed at 95 °C for 60 min. The leaves extract was filtered through Whatman qualitative filter paper No. 1 and centrifuged at 5000 rpm for 5 min to remove large particles. To prevent thermal destruction of the filtered extract, it was kept at 4 °C to be used in the preparation of nanomaterials [26].

## 2.3 Preparation of the nanomaterials

### 2.3.1 Synthesis of ZnO (ext)

A simple microwave oven (2.45 GHz and 1000 W) was applied for green synthesis of ZnO using *M. longifolia* leaf extract (ZnO (ext)). In this method, 7.31 g zinc (II) nitrate was dissolved in a solution with a volume ratio 20 mL of the extract and 80 mL of DW. In order to adjust pH to 10, an aqueous solution of NaOH (5 M) was drop-wisely added into the solution under stirring. Then, the suspension was irradiated for 10 min in the microwave oven. The resultant light brown precipitate was separated from the reaction suspension by centrifugation at 5000 rpm for 8 min. Then, it was washed with DW and ethanol repeatedly and oven-dried at 60 °C for 24 h.

### 2.3.2 Synthesis of ZnO (W)

The ZnO sample in water, ZnO (W), was prepared with the same procedure, except that zinc nitrate was dissolved into 100 mL of DW. Briefly, 7.31 g zinc (II) nitrate was dissolved in 100 mL of DW. After that, using an aqueous solution of NaOH (5 M), it was adjusted to pH 10. Then, the suspension was irradiated for 10 min in the microwave oven. Thereafter, the resultant white precipitate was separated by centrifugation and it was washed with DW and ethanol and finally was dried at 60 °C for 24 h.

### 2.3.3 Synthesis of ZnO/CuO

In the case of the ZnO/CuO (10%) nanocomposite, 1.644 g zinc nitrate and 0.1254 g copper acetate were dissolved in 80 mL DW and 20 mL of the leaf extract. The pH of the solution was adjusted to 10 by drop wise adding an aqueous solution of NaOH (5 M), and afterward it was irradiated for 10 min in the microwave oven. The formed precipitate was separated from the reaction suspension by centrifugation and it was washed and dried similar to that of ZnO. For preparation of the ZnO/CuO (5%) nanocomposite, the amounts of zinc nitrate and copper acetate were 3.47 and 0.152 g,

respectively. The schematic diagram for preparation of the samples is illustrated in Scheme 1.

## 2.4 Instruments

The XRD patterns were used for determination of the crystallinity and average crystallite sizes of the samples, which provided by a Philips Xpert X-ray diffractometer with Cu K $\alpha$  radiation ( $\lambda=0.15406$  nm). Morphology of the samples and surface morphology of the bacteria were observed with LEO 1430VP SEM, using an accelerating voltage of 15 kV. Compositions of the samples were analyzed with an EDX system on the same SEM. The TEM images were obtained by means of a CM30 Philips, using an acceleration voltage of 150 kV. TGA of the samples was obtained using Linseis STAPT 1000 by heating under air atmosphere from room temperature to 700 °C at 10 °C/min. The FT-IR analysis was performed by a Perkin Elmer Spectrum RX I apparatus. UV–Vis DR spectra were recorded by a Scinco 4100 apparatus. Textural properties of the samples were investigated by a Micromeritics Tristar II Plus adsorption apparatus at  $-196$  °C.

## 2.5 Anti-bacterial activity assessment

Anti-bacterial activity of the as-prepared samples against *E. coli* and *S. aureus* was assessed using colony forming units (CFU) enumeration method [27, 28]. The bacteria were cultured in 50 mL of NB and incubated at 37 °C. The cell concentration was adjusted to  $10^7$  CFU mL $^{-1}$  in the reaction solution. Different concentrations of the fabricated samples were prepared in the sterilized NB medium in a final volume of 3 mL. The growth of bacteria was monitored without and with nanomaterials at an optimized concentration of 128  $\mu$ g mL $^{-1}$ . Subsequently, the cultures were incubated in a shaker incubator for 24 h at 190 rpm min $^{-1}$  and at 37 °C.

Afterwards, the optical density was measured at 600 nm. The agar plates were then surface inoculated with 100  $\mu$ L of each bacterial suspension. The plates were incubated at 37 °C for 48 h and the number of viable colonies was counted for each isolate in triplicate.

## 3 Results and discussion

### 3.1 Characterization

Figure 1 shows XRD patterns obtained for the ZnO (W), ZnO (ext), ZnO/CuO (5%), and ZnO/CuO (10%) samples. For the ZnO (W) and ZnO (ext) samples, all of the peaks were corresponding to hexagonal crystalline phase of ZnO (JCPDS card No. 36-1451) [29, 30]. The Scherrer's equation

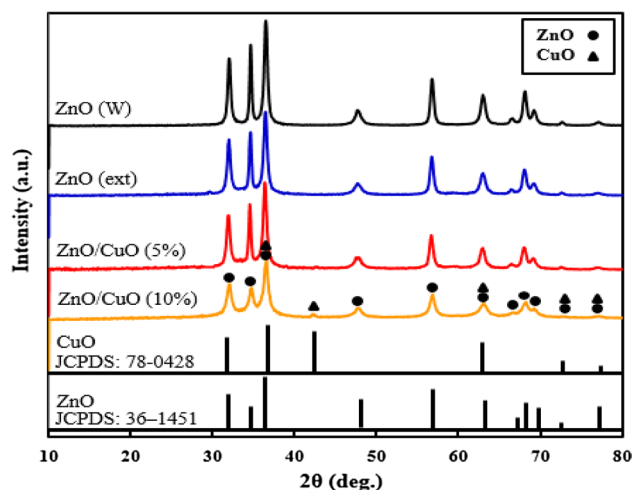
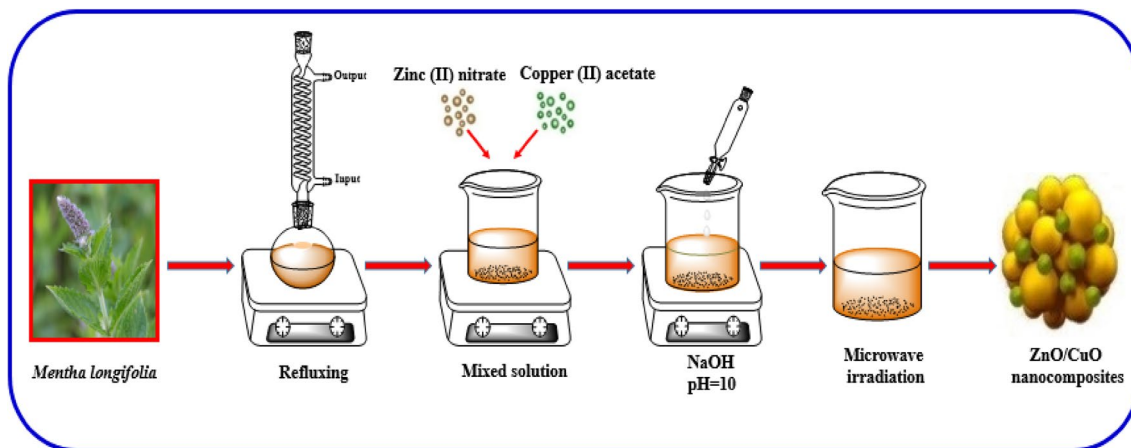


Fig. 1 XRD patterns for the ZnO (W), ZnO (ext), ZnO/CuO (5%), and ZnO/CuO (10%) samples



Scheme 1 The schematic diagram for synthesis of the ZnO/CuO nanocomposites

**Table 1** Average crystallite sizes for ZnO and CuO in the as-prepared samples

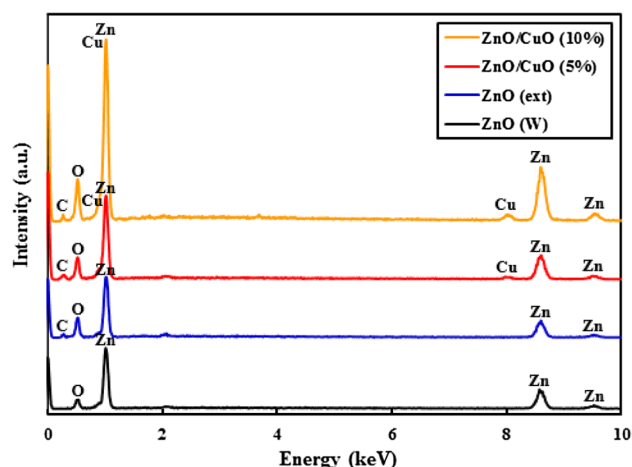
Semiconductor	Average crystallite size (nm)			
	ZnO (W)	ZnO (ext)	ZnO/CuO (5%)	ZnO/CuO (10%)
ZnO	29	24	16	14
CuO	–	–	11	10

(Eq. 1) was applied to calculate the average crystallite size of the prepared samples [26].

$$D = K\lambda/\beta \cos \theta \quad (1)$$

where  $K$  is Scherrer's constant, which is 0.9, wavelength of X-ray radiation is  $\lambda = 0.15406$  nm,  $\beta$  is peak width at half maximum, and  $\theta$  is Bragg's angle. Hence, the average crystallite sizes for the all samples were calculated and reported in Table 1. As seen, size of the particles for the ZnO sample fabricated in the presence of the extract is lower than that of the sample prepared in water. As known, different functional groups including C–O, C=O, and O–H presented in the leaf extract of *M. longifolia*, which are related to biocompounds such as phenolic compounds and flavonoids. Molecules of these compounds stabilize particles of ZnO during their growth, which is responsible for stabilization and formation of smaller particles of the ZnO (ext) sample in comparison with the ZnO (W) sample [31, 32]. Similar results have been observed during fabrication of ZnO particles in the presence of various plant extracts [33, 34]. Furthermore, in the ZnO/CuO (5%) and ZnO/CuO (10%) nanocomposites, other than the peaks of hexagonal crystalline phase of ZnO, the reflection peaks of CuO with low intensity were observed, according to its low weight percentages. The observed peaks of CuO were attributed to the cubic crystallite phase (JCPDS card No. 78–0428) [35].

In this step, EDX analysis was exploited to evaluate chemical composition and purity of the ZnO (W), ZnO (ext), ZnO/CuO (5%), and ZnO/CuO (10%) samples, as shown in Fig. 2. The EDX spectra revealed the presence of zinc and oxygen elements for the ZnO (W) sample. The ZnO (ext) sample exhibited zinc, oxygen, and carbon elements. Additionally, the EDX spectra for the ZnO/CuO (5%) and ZnO/CuO (10%) nanocomposites, revealed the presence of zinc, oxygen, carbon, and copper elements. The presence of carbon element in the EDX spectra of these samples were ascribed to binding different biomolecules from the leaf extract to the surface of the fabricated ZnO [25]. Moreover, according to the results, no impurity peaks were detected, which indicated high purity of the fabricated samples. The weight percentages of Zn and O elements in the ZnO (W) sample were 86.7, and 13.3%, respectively. Furthermore, in

**Fig. 2** EDX spectra for the ZnO (W), ZnO (ext), ZnO/CuO (5%), and ZnO/CuO (10%) samples

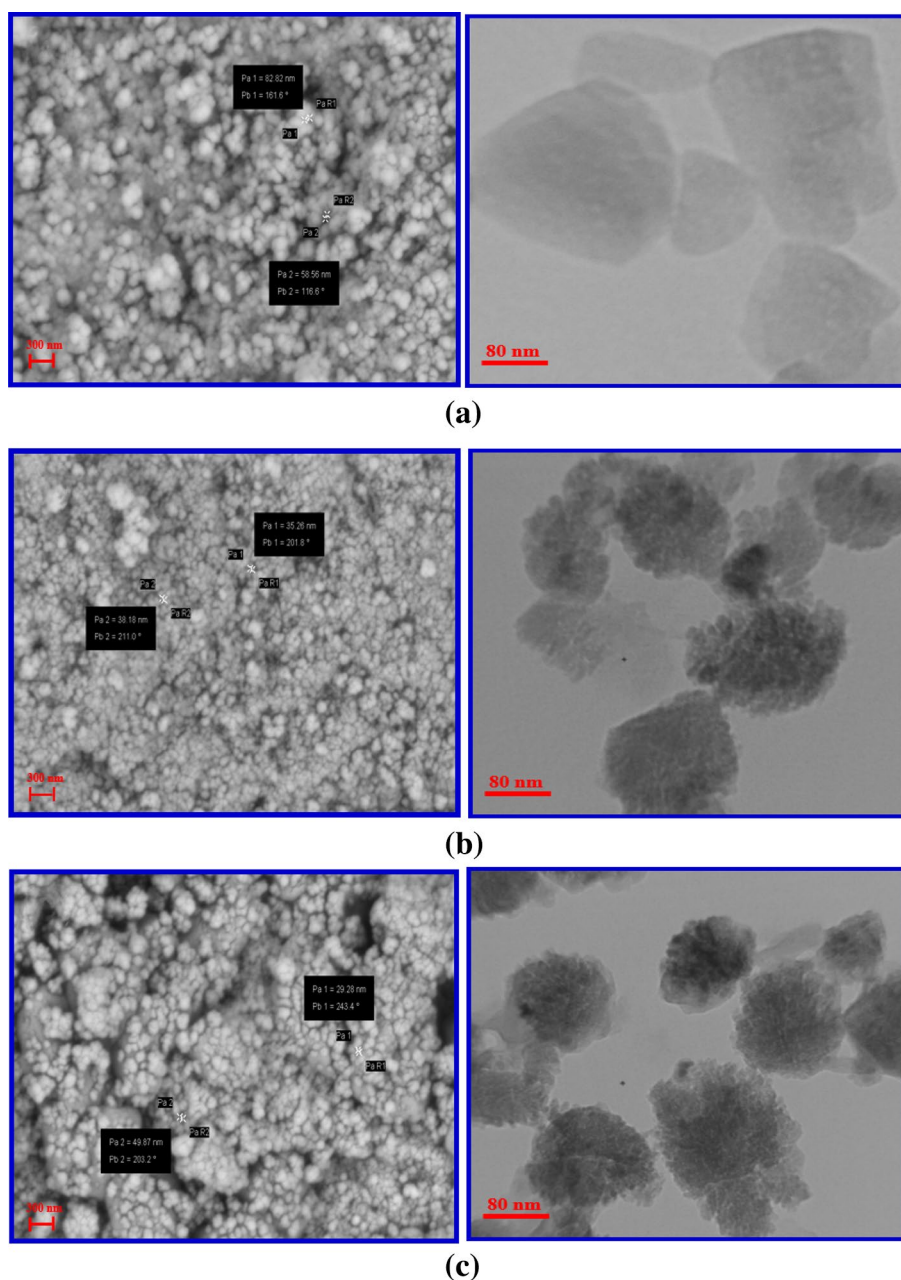
the ZnO (ext) sample, the weight percentages of Zn, O, and C elements were obtained as 79.7, 19.0, and 1.30%, respectively. Weight percentages of Zn, O, C, and Cu elements in the ZnO/CuO (5%) nanocomposite were found to be 72.1, 21.4, 2.40, and 4.1%, respectively. Finally, the weight percentages of Zn, O, C, and Cu elements in the ZnO/CuO (10%) nanocomposite were found to be 73.2, 19.2, 2.3, and 5.3%, respectively.

Morphology of the ZnO (W), ZnO (ext), and ZnO/CuO (5%) samples were studied using SEM and TEM instruments and their images are shown in Fig. 3. As observed, in all samples, the most of particles are nearly spherical. Additionally, for the ZnO (ext) and ZnO/CuO (5%) samples, prepared in the presence of the leaf extract, mean particle sizes were decreased, which were in accordance with the results of the XRD analysis.

TG analysis was performed to determine thermal stability and weight percentages of the binded leaf extract over the samples. Figure 4 shows the TGA plots for the ZnO (W), ZnO (ext), ZnO/CuO (5%), and ZnO/CuO (10%) nanocomposite. As observed, the ZnO (W) sample showed a weight loss of 1.4% after heating up to 700 °C. This decrease was ascribed to desorption of water molecules adsorbed over the sample. In the case of the ZnO (ext), ZnO/CuO (5%), and ZnO/CuO (10%) samples, the weight loss, by heating up to about 200 °C, was attributed to the dehydration step, similar to the ZnO (W) sample. However, by further heating of these samples, much more decreases in the weights were observed. These decreases were related to the burning of the organic molecules from the leaf extract binded to the surface of these samples. Weight percentages of organic contents of the ZnO (ext), ZnO/CuO (5%), and ZnO/CuO (10%) samples were calculated from the weights remained after heating the samples up to 650 °C. Weight percentages



**Fig. 3** SEM and TEM images for the prepared samples: **a** ZnO (W), **b** ZnO (ext), and **c** ZnO/CuO (5%)



of the biomolecules in the ZnO (ext), ZnO/CuO (5%), and ZnO/CuO (10%) samples were calculated to be 17, 17.5%, and 22.2% respectively. Similar results have been reported for TG analysis of the ZnO particles fabricated in the presence of different plant extracts [36–38].

FT-IR spectra were also recorded to determine the functional groups of the samples in the range of 400–4000  $\text{cm}^{-1}$ . The FT-IR spectra of the leaf extract and prepared samples are shown in Fig. 5. The spectra of ZnO (W), ZnO (ext), ZnO/CuO (5%), and ZnO/CuO (10%) samples exhibited a peak in wavenumber of 476  $\text{cm}^{-1}$ , which was ascribed to the stretching vibration of Zn–O bond [39, 40]. The ZnO/CuO (5%) and ZnO/CuO (10%) samples showed a distinct

peak at 564  $\text{cm}^{-1}$ , which was related to the Cu–O bond [41, 42]. In addition, the peaks at 1073 and 1623  $\text{cm}^{-1}$  were attributed to stretching vibrations of the C–O and C=O bonds from the biomolecules presented in the leaf extract [43, 44]. The absorption peaks for C–H stretching vibrations of  $\text{CH}_2$  and  $\text{CH}_3$  groups were observed at 2862 and 2934  $\text{cm}^{-1}$ , respectively [45]. Finally, the FT-IR spectra of the leaf extract and all samples showed broad absorption peaks at 3200–3668  $\text{cm}^{-1}$ , representing stretching vibration of O–H group [46].

UV–Vis DR spectra could provide useful information about the electronic absorption properties of the samples. Hence, the UV–Vis spectra of the resultant ZnO (W), ZnO

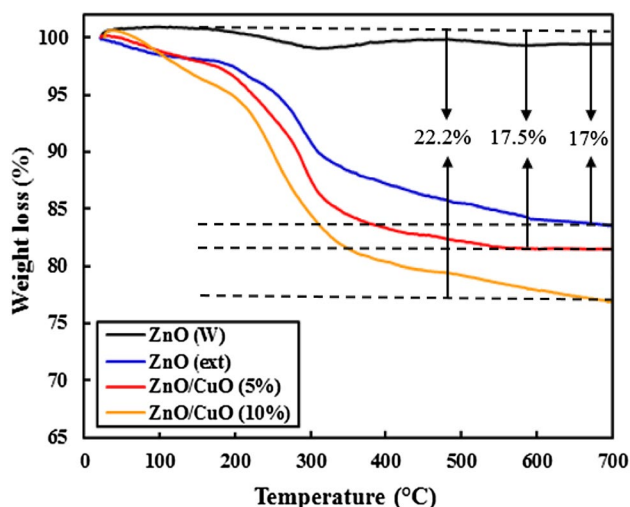
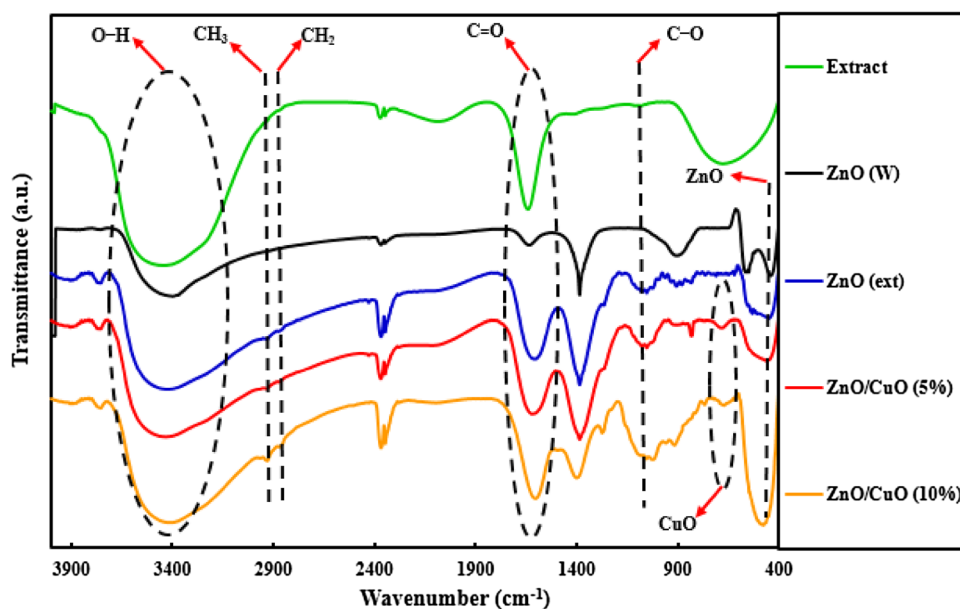


**Fig. 4** TGA analysis for the ZnO (W), ZnO (ext), ZnO/CuO (5%), and ZnO/CuO (10%) samples

(ext), ZnO/CuO (5%), and ZnO/CuO (10%) samples were obtained, and the results are shown in Fig. 6. As seen, the ZnO (W) sample showed an intensive absorption only in UV region with a sharp peak at 370 nm. Interestingly, the ZnO (ext) sample displayed absorptions in UV and visible regions. The characteristic peak in UV region of the ZnO (ext) sample showed a distinct blue shift of 41 nm. This shift in the absorption peak was related to decrease of the particle sizes for the ZnO sample prepared in the presence of the leaf extract, which is attributed to the quantum confinement effect [31]. When materials are as small as nanoscale, their properties deviate considerable from the properties in bulk materials. At this scale, band gap energy of semiconductor

**Fig. 5** FT-IR spectra for the *M. longifolia* leaf extract, ZnO (W), ZnO (ext), ZnO/CuO (5%), and ZnO/CuO (10%) samples



increases and becomes size dependent and a blue shift in the electronic spectra is observed [47]. Furthermore, the ZnO (ext), ZnO/CuO (5%), and ZnO/CuO (10%) samples had strong absorption in visible region due to the presence of biomolecules from the leaf extract. Therefore, the results obtained from the DRS data were parallel with the EDX, TGA, and FT-IR analyses, confirming the presence of biomolecules from the leaf extract adsorbed over the as-prepared samples.

The BET surface areas and pore properties of the ZnO (W), ZnO (ext), ZnO/CuO (5%), and ZnO/CuO (10%) samples were explored by using nitrogen adsorption–desorption isotherms. The results of these analyses are shown in Fig. 7 and the calculated parameters are reported in Table 1. The BET results revealed that the samples showed typical IV isotherms, indicating the fact that they almost have mesopore structures [48]. The calculated specific surface areas for the ZnO (W), ZnO (ext), ZnO/CuO (5%), and ZnO/CuO (10%) samples were 29.3, 43.0, 36.0 and 26.0 m<sup>2</sup> g<sup>-1</sup>, respectively. Moreover, total pore volumes of the ZnO (W), ZnO (ext), ZnO/CuO (5%), and ZnO/CuO (10%) samples were 0.1981, 0.2003, 0.0939, and 0.0984 cm<sup>3</sup> g<sup>-1</sup>, respectively. The decrease of the textural properties for the ZnO/CuO samples is attributed to the blocking of the surface active sites by CuO particles (Table 2).

### 3.2 Anti-bacterial activity investigations

Anti-bacterial activity of the ZnO (W), ZnO (ext), ZnO/CuO (5%), and ZnO/CuO (10%) samples against *E. coli* and *S. aureus* was investigated at an optimized concentration of 128 μg mL<sup>-1</sup> using CFU enumeration method. Figures 8 and 9 show the results of anti-bacterial activities of the prepared

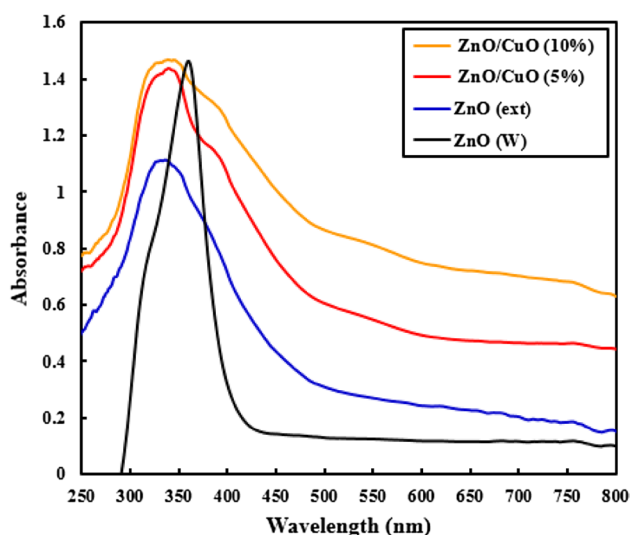


**Fig. 6** UV-Vis DRS spectra for the ZnO (W), ZnO (ext), ZnO/CuO (5%), and ZnO/CuO (10%) samples

**Table 2** Specific surface area and pore properties for the ZnO (W), ZnO (ext), ZnO/CuO (5%), and ZnO/CuO (10%) samples

Sample	Surface area ( $\text{m}^2 \text{g}^{-1}$ )	Mean pore diameter (nm)	Total pore volume ( $\text{cm}^3 \text{g}^{-1}$ )
ZnO (W)	29.3	27.0	0.1981
ZnO (ext)	43.0	19.0	0.2003
ZnO/CuO (5%)	36.0	10.5	0.0939
ZnO/CuO (10%)	26.0	15.0	0.0984

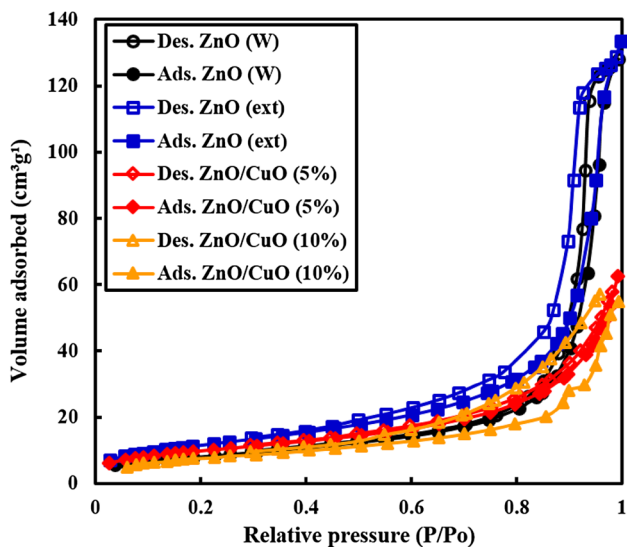


**Fig. 7** Nitrogen adsorption–desorption plots for the ZnO (W), ZnO (ext), ZnO/CuO (5%), and ZnO/CuO (10%) samples

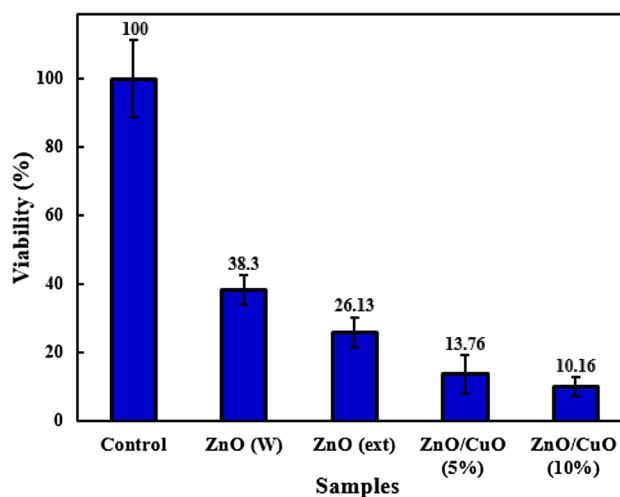


**Fig. 8** Anti-bacterial activity of the prepared samples against *E. coli* bacteria

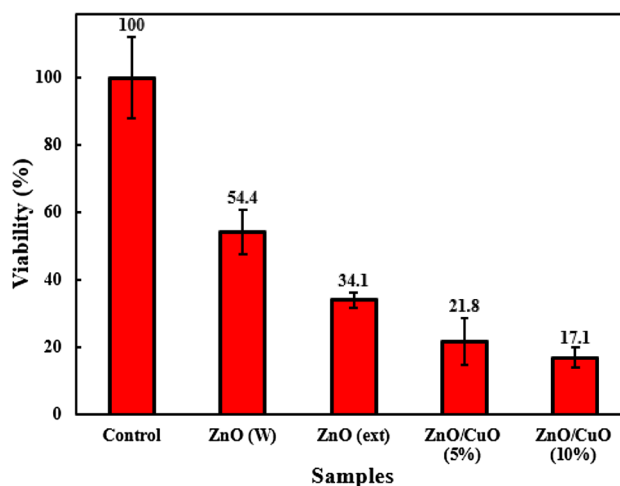


**Fig. 9** Anti-bacterial activity of the prepared samples against *S. aureus* bacteria

samples against the pathogenic bacteria. The differences in the viability of these bacteria were statistically significant by one-way ANOVA at  $P < 0.05$ , as indicated. As observed, the anti-bacterial activities are significantly different among experimental groups and the control group. Furthermore, the anti-bacterial activities of the ZnO (W) sample against both pathogenic bacteria were less than those of other samples. When ZnO was synthesized using the leaf extract, the viability percentages of the bacteria were reduced. Besides, the results obviously demonstrated strong anti-bacterial activities for the ZnO/CuO nanocomposites. Furthermore, the viability percentages of the pathogenic bacteria in the presence of the ZnO/CuO (5%) nanocomposite was significantly reduced by increasing the CuO content. For this reason, the ZnO/CuO nanocomposites displayed substantial

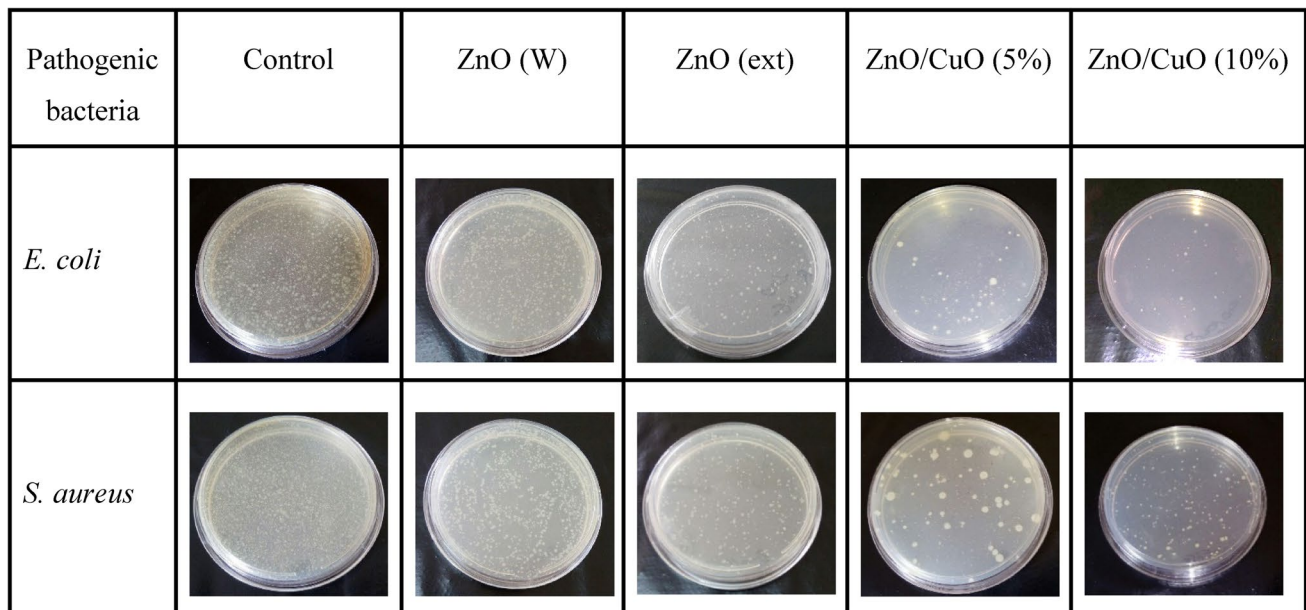


**Fig. 10** Anti-bacterial activities of the ZnO (W), ZnO (ext), ZnO/CuO (5%), and ZnO/CuO (10%) samples against *E. coli* and *S. aureus*

anti-bacterial activity. Finally, it is observed that the anti-bacterial activity of ZnO/CuO (10%) nanocomposite against *E. coli* ( $10.16 \pm 2.2$ ) was higher than that observed for *S. aureus* ( $17.1 \pm 0.87$ ).

For better insights, the pathogenic bacteria were inactivated with the prepared samples and their optical images are illustrated in Fig. 10. As it is obvious, the highest anti-bacterial activity belonged to the ZnO/CuO (10%) nanocomposite and the other compounds, including ZnO/CuO (5%), ZnO (ext), and ZnO (W) were in the next ranks, respectively. Furthermore, in all samples, the number of cell colonies for *E. coli* were less than those for *S. aureus*. Thus, in accordance with the viability percentages, these images supported enhanced anti-bacterial activity for the prepared samples in the presence of the leaf extract.

According to the related literature, cell damage, oxidative stress phenomena, and genomic and plasmid DNA degradation are plausible factors that can kill bacteria [49–52]. In order to determine the mechanism for anti-bacterial activity of the ZnO/CuO (10%) nanocomposite, the surface morphologies of both *E. coli* and *S. aureus* bacteria were investigated by SEM, as the images are shown in Fig. 11. According to Fig. 11a, b for *E. coli* bacteria, the SEM images clearly revealed wrinkled bacterial membranes and obvious cracks on the cell surfaces. In addition, as shown in Fig. 11c, d, the ZnO/CuO (10%) nanocomposite ruptured the outer and inner membrane of the *S. aureus* cells, resulting in the disorganization of cell wall and secretion of the inner content [53, 54].

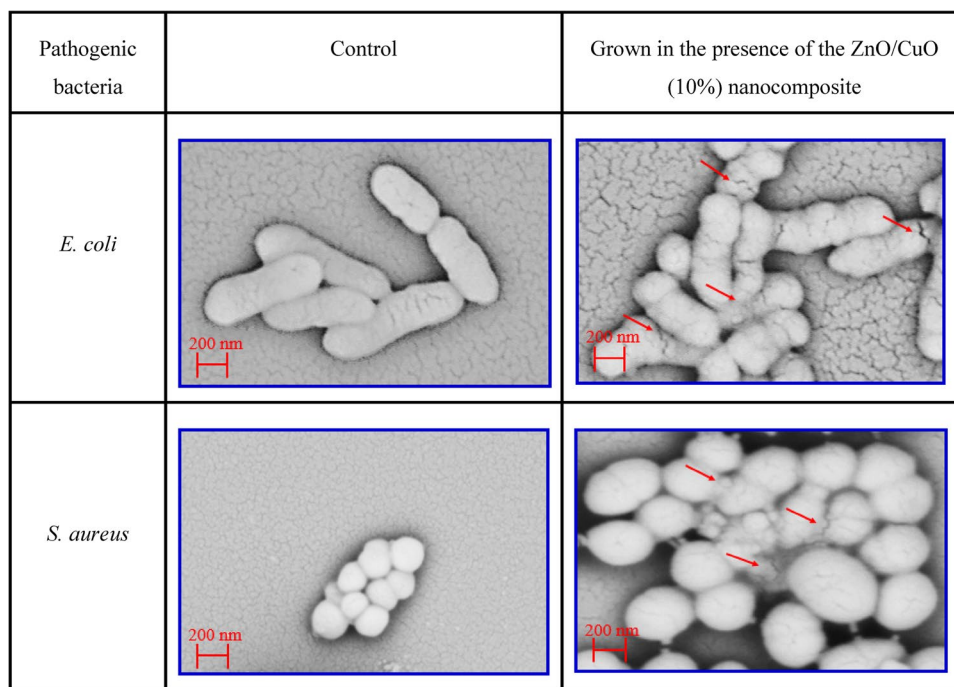
In contrast, a little morphological changes were observed in the SEM images of *E. coli*.

## 4 Conclusion

The present study focused on the development of a green, fast, and simple microwave-assisted method for synthesis of the ZnO and ZnO/CuO nanocomposites, using the leaf extract of a medicinal plant, *M. longifolia*. According to the XRD and EDX results, no impurity peaks were detected, which indicated high purity of the fabricated samples. In addition, the XRD analysis indicated that the mean size of crystallites was decreased for the ZnO powder prepared in the presence of the extract. From the SEM images, the spherical shape and well-distribution of the particles were observed. The EDX, TGA, UV–Vis DRS, and FT-IR analyses confirmed the existence of biomolecules from *M. longifolia* leaf extract bound over the prepared samples. Furthermore, results indicated, when samples were synthesized using the leaf extract, the viability percentages of the bacteria were reduced. Moreover, the SEM images of the bacteria confirmed the mechanism for anti-bacterial activity of the ZnO/CuO (%10) nanocomposite. Finally, our results indicated that Gram-negative bacterial strains were more sensitive in comparison to Gram-positive strains against the tested nanocomposites, and disclosed the potential application of the nanocomposites as appropriate candidates for successful minimization of bacterial infections that may occur.



**Fig. 11** SEM images of the pathogenic bacteria (control and grown in the presence of the ZnO/CuO (10%) nanocomposite)



**Acknowledgements** This study was financially supported by University of Mohaghegh Ardabili.

## References

1. S. Mihindukulasuriya, L.T. Lim, Nanotechnology development in food packaging: a review. *Trends Food Sci. Technol.* **40**, 149–167 (2014)
2. P. Palmero, Structural ceramic nanocomposites: a review of properties and powders' synthesis methods. *Nanomaterials* **5**, 656–696 (2015)
3. K. Müller, E. Bugnicourt, M. Latorre, M. Jorda, Y.S. Echegoyen, J.M. Lagaron, O. Miesbauer, A. Bianchin, S. Hankin, U. Böhlz, G. Pérez, M. Jesdinski, M. Lindner, Z. Scheuerer, S. Castelló, M. Schmid, Review on the processing and properties of polymer nanocomposites and nanocoatings and their applications in the packaging, automotive and solar energy fields. *Nanomaterials* **7**, 1–74 (2017)
4. S. Ahmed, S.A. Chaudhry, S. Ikram, A review on biogenic synthesis of ZnO nanoparticles using plant extracts and microbes: a prospect towards green chemistry. *J. Photochem. Photobiol. B* **166**, 272–284 (2017)
5. A.B. Djurišić, X. Chen, Y.H. Leung, A.M.C. Ng, ZnO nanostructures: Growth, properties and applications. *J. Mater. Chem.* **22**, 6526–6535 (2012)
6. K. Qi, B. Cheng, J. Yu, W. Ho, Review on the improvement of the photocatalytic and antibacterial activities of ZnO. *J. Alloy. Compd.* **727**, 792–820 (2017)
7. R. Kumar, A. Umar, G. Kumar, H.S. Nalwa, Antimicrobial properties of ZnO nanomaterials: a review. *Ceram. Int.* **43**, 3940–3961 (2017)
8. C.B. Ong, L.Y. Ng, A.W. Mohammad, A review of ZnO nanoparticles as solar photocatalysts: synthesis, mechanisms and applications. *Renew. Sustain. Energy Rev.* **81**, 536–551 (2018)
9. A.P. Ingle, N. Duran, M. Rai, Bioactivity, mechanism of action, and cytotoxicity of copper-based nanoparticles: a review. *Appl. Microbiol. Biotechnol.* **98**, 1001–1009 (2014)
10. I. Hussain, N. Singh, A. Singh, H. Singh, S. Singh, Green synthesis of nanoparticles and its potential application. *Biotechnol. Lett.* **38**, 545–560 (2016)
11. J. Singh, G. Kaur, M. Rawat, A brief review on synthesis and characterization of copper oxide nanoparticles and its applications. *J. Bioelectron Nanotechnol.* **1**, 1–9 (2016)
12. J.R.P. Videia, Y. Huang, J.G. Parsons, L. Zhao, L.L. Moreno, J.A.H. Viezcas, J.L.G. Torresdey, Plant-based green synthesis of metallic nanoparticles: scientific curiosity or a realistic alternative to chemical synthesis? *Nanotechnol. Environ. Eng.* **4**, 1–29 (2016)
13. A. Dey, Semiconductor metal oxide gas sensors: a review. *Mater. Sci. Eng. B* **229**, 206–217 (2017)
14. C. Su, Environmental implications and applications of engineered nanoscale magnetite and its hybrid nanocomposites: a review of recent literature. *J. Hazard. Mater.* **322**, 48–84 (2017)
15. B. Boro, B. Gogoi, B.M. Rajbongshi, A. Ramchiary, Nano-structured TiO<sub>2</sub>/ZnO nanocomposite for dye-sensitized solar cells application: a review. *Renew. Sustain. Energy Rev.* **81**, 2264–2270 (2017)
16. L.S. Sundar, K.V. Sharma, M.K. Singh, A.C.M. Sousa, Hybrid nanofluids preparation, thermal properties, heat transfer and friction factor—a review. *Renew. Sustain. Energy Rev.* **68**, 185–198 (2017)
17. M.B. Gawande, S.N. Shelke, R. Zboril, R.S. Varma, Microwave-assisted chemistry: Synthetic applications for rapid assembly of nanomaterials and organics. *Acc. Chem. Res.* **47**, 1338–1348 (2014)
18. A.K. Rathi, M.B. Gawande, R. Zboril, R.S. Varma, Microwave-assisted synthesis—catalytic applications in aqueous media. *Coord. Chem. Rev.* **291**, 68–94 (2015)
19. S. Ahmed, M. Ahmad, B.L. Swami, S. Ikram, A review on plants extract mediated synthesis of silver nanoparticles for antimicrobial applications: a green expertise. *J. Adv. Res.* **7**, 17–28 (2015)

20. U. Shanker, V. Jassal, M. Rani, B.S. Kaith, Towards green synthesis of nanoparticles: from bio-assisted sources to benign solvents. a review. *Int. J. Environ. Anal. Chem.* **96**, 801–835 (2016)
21. R. Harley, C. Brighton, Chromosome numbers in the genus *Mentha* L. *Bot. J. Linn. Soc.* **74**, 71–96 (1977)
22. B.M. Lange, R. Croteau, Genetic engineering of essential oil production in mint. *Curr. Opin. Plant Biol.* **2**, 139–144 (1999)
23. A.R. Andro, D. Atofani, I. Boz, M. Zamfirache, I. Burzo, C. Toma, Studies concerning the histo-anatomy and biochemistry of *Mentha longifolia* L. Huds. during vegetative phenophase. *Analele Stiintifice ale Universitatii "Al I Cuza" din Iasi* **57**, 25–30 (2011)
24. P. Mikaili, S. Mojaverrostami, M. Moloudizargari, S. Aghajanshakeri, Pharmacological and therapeutic effects of *Mentha Longifolia* L. and its main constituent, menthol. *Anc. Sci. Life* **33**, 115–131 (2013)
25. A. Ertas, A.C. Gören, N. Hasimi, V. Tolan, U. Kolak, Evaluation of antioxidant, cholinesterase inhibitory and antimicrobial properties of *Mentha longifolia* subsp. noeana and its secondary metabolites. *Rec. Nat. Prod.* **9**, 105–115 (2015)
26. V.V. Gawade, N.L. Gavade, H.M. Shinde, S.B. Babar, A.N. Kadam, K.M. Garadkar, Green synthesis of ZnO nanoparticles by using *Calotropis procera* leaves for the photodegradation of methyl orange. *J. Mater. Sci.* **28**, 14033–14039 (2017)
27. B. Gao, S. He, J. Guo, R. Wang, Preparation and antibacterial character of a water-insoluble antibacterial material of grafting polyvinylpyridinium on silica gel. *Mater. Lett.* **61**, 877–883 (2007)
28. S.C. Fernandes, P. Sadocco, A.A. Varona, T. Palomares, A. Eceiza, A.J. Silvestre, I. Mondragon, C.S.R. Freire, Bioinspired antimicrobial and biocompatible bacterial cellulose membranes obtained by surface functionalization with aminoalkyl groups. *ACS Appl. Mater. Interfaces* **5**, 3290–3297 (2013)
29. A. Omid, A. Habibi-Yangjeh, M. Pirhashemi, Application of ultrasonic irradiation method for preparation of ZnO nanostructures doped with Sb + 3 ions as a highly efficient photocatalyst. *Appl. Surf. Sci.* **276**, 468–475 (2013)
30. P.A. Luque, C.A. Soto Robles, O. Nava, C.M. Gómez Gutierrez, A. Castro-Beltran, E. Garrafa-Galvez, A.R. Vilchis-Nestor, A. Olivas, Green synthesis of zinc oxide nanoparticles using *Citrus sinensis* extract. *J. Mater. Sci.* (2018). <https://doi.org/10.1007/s10854-018-9015-2>
31. K. Elumalai, S. Velmurugan, S. Ravi, V. Kathiravan, S. Ashokkumar, Green synthesis of zinc oxide nanoparticles using *Moringa oleifera* leaf extract and evaluation of its antimicrobial activity. *Elsevier* **134**, 158–164 (2015)
32. B. Siripreddy, B.K. Mandal, Facile green synthesis of zinc oxide nanoparticles by *Eucalyptus globulus* and their photocatalytic and antioxidant activity. *Adv. Powder Technol.* **28**, 785–797 (2017)
33. P. Vanathi, P. Rajiv, S. Narendhran, S. Rajeshwari, P.K. Rahman, R. Venkatesh, Biosynthesis and characterization of phyto mediated zinc oxide nanoparticles: a green chemistry approach. *Mater. Lett.* **134**, 13–15 (2014)
34. M. Ramesh, M. Anbuvarannan, G. Viruthagiri, Green synthesis of ZnO nanoparticles using *Solanum nigrum* leaf extract and their antibacterial activity. *Spectrochim. Acta Part A* **134**, 864–870 (2015)
35. M. Kuznetsov, M. Mafina, O. Belousova, N. Vakin, S. Shchupkin, I. Morozov, Catalytically active magnetic nanoparticles in the Cu-O system. *Inorg. Mater.* **51**, 307–318 (2015)
36. P. Nagajyothi, T. Sreekanth, C.O. Tettey, Y.I. Jun, S.H. Mook, Characterization, antibacterial, antioxidant, and cytotoxic activities of ZnO nanoparticles using *Coptidis Rhizoma*. *Bioorg. Med. Chem. Lett.* **24**, 4298–4303 (2014)
37. H. Padalia, S. Baluja, S. Chanda, Effect of pH on size and antibacterial activity of *Salvadora oleoides* leaf extract-mediated synthesis of zinc oxide nanoparticles. *BioNanoScience* **7**, 40–49 (2017)
38. R. Mohammadi-Aloucheh, A. Habibi-Yangjeh, A. Bayrami, S. Latifi-Navid, A. Asadi, Enhanced anti-bacterial activities of ZnO nanoparticles and ZnO/CuO nanocomposites synthesized using *Vaccinium arctostaphylos* L. fruit extract. *Artif Cells Nanomed. Biotechnol.* (2018). <https://doi.org/10.1080/21691401.2018.1448988>
39. A. Azam, A.S. Ahmed, M. Oves, M.S. Khan, S.S. Habib, A. Memic, Antimicrobial activity of metal oxide nanoparticles against Gram-positive and Gram-negative bacteria: a comparative study. *Int. J. Nanomed.* **7**, 6003–6009 (2012)
40. S. Jafarirad, M. Mehrabi, B. Divband, M. Kosari-Nasab, Biofabrication of zinc oxide nanoparticles using fruit extract of *Rosa canina* and their toxic potential against bacteria: a mechanistic approach. *Mater. Sci. Eng. C* **59**, 296–302 (2016)
41. J. Jayaprakash, N. Srinivasan, P. Chandrasekaran, E. Girija, Synthesis and characterization of cluster of grapes like pure and Zinc-doped CuO nanoparticles by sol-gel method. *Spectrochim. Acta Part A* **136**, 1803–1806 (2015)
42. B.G. Mahmoud, M. Khairy, F.A. Rashwan, C.W. Foster, C.E. Banks, Self-assembly of porous copper oxide hierarchical nanostructures for selective determinations of glucose and ascorbic acid. *RSC Adv.* **6**, 14474–14482 (2016)
43. F.A. Al-Bayati, Isolation and identification of antimicrobial compound from *Mentha longifolia* L. leaves grown wild in Iraq. *Ann. Clin. Microbiol. Antimicrob.* **8**, 1–6 (2009)
44. E.A. Petrakis, A.C. Kimbaris, C.S. Pappas, P.A. Tarantilis, M.G. Polissiou, Quantitative determination of pulegone in pennyroyal oil by FT-IR spectroscopy. *J. Agric. Food Chem.* **57**, 10044–10048 (2009)
45. D.M. Pramila, R. Xavier, K. Marimuthu, S. Kathiresan, M.L. Khoo, M. Senthilkumar, K. Sathya, S. Sreeramanan, Phytochemical analysis and antimicrobial potential of methanolic leaf extract of peppermint (*Mentha piperita*: Lamiaceae). *J. Med. Plants Res.* **6**, 331–335 (2012)
46. H.S. Kadhemi, H.J.M. AL-Mathkhury, Inhibitory effect of menthol extracted from *Mentha rubra* on methicillin-resistant *Staphylococcus aureus*. *World J. Exp. Biosci.* **3**, 150–154 (2015)
47. T.A. Para, V. Shelke, Extreme blue-shifted photoluminescence from quantum confinement of core-shell ZnO. *J. Mater. Sci.* **24**, 18842–18848 (2017)
48. M. Pirhashemi, A. Habibi-Yangjeh, Photosensitization of ZnO by AgBr and Ag<sub>2</sub>CO<sub>3</sub>: nanocomposites with tandem nn heterojunctions and highly enhanced visible-light photocatalytic activity. *J. Colloid Interface Sci.* **474**, 103–113 (2016)
49. L. Zhang, Y. Jiang, Y. Ding, N. Daskalakis, L. Jeuken, M. Povey, A.J.O. Neill, D.W. York, Mechanistic investigation into antibacterial behaviour of suspensions of ZnO nanoparticles against *E. coli*. *J. Nanoparticle Res.* **12**, 1625–1636 (2010)
50. K. Elumalai, S. Velmurugan, Green synthesis, characterization and antimicrobial activities of zinc oxide nanoparticles from the leaf extract of *Azadirachta indica* (L.). *Appl. Surf. Sci.* **345**, 329–336 (2015)
51. S. Ambika, M. Sundrarajan, Antibacterial behaviour of *Vitex negundo* extract assisted ZnO nanoparticles against pathogenic bacteria. *J. Photochem. Photobiol. B* **146**, 52–57 (2015)
52. G. Krithika, R. Saraswathy, M. Muralidhar, D. Thulasi, N. Lalitha, P. Kumararaja, A. Nagavel, A. Balaji, R. Jayavel, Zinc oxide nanoparticles-synthesis, characterization and antibacterial activity. *J. Nanosci. Nanotechnol.* **17**, 5209–5216 (2017)
53. T. Bhuyan, K. Mishra, M. Khanuja, R. Prasad, A. Varma, Biosynthesis of zinc oxide nanoparticles from *Azadirachta indica* for antibacterial and photocatalytic applications. *Mater. Sci. Semicond. Process.* **32**, 55–61 (2015)
54. N. Bala, S. Saha, M. Chakraborty, M. Maiti, S. Das, R. Basu, P. Nandy, Green synthesis of zinc oxide nanoparticles using *Hibiscus subdariffa* leaf extract: effect of temperature on synthesis, anti-bacterial activity and anti-diabetic activity. *RSC Adv.* **5**, 4993–5003 (2015)